Kinetic features of ethanol steam reforming and decomposition using a biochar-supported Ni catalyst

Ahmed Tijani F. Afolabi,[a, b] Panagiotis N. Kechagiopoulos,[b,*] Yurong Liu,[a] Chun-Zhu Li[a, *]

[a] Fuels and Energy Technology Institute, Curtin University, GPO Box U1987, Perth, WA 6845, Australia
[b] Chemical and Materials Engineering Group, School of Engineering, University of Aberdeen, Aberdeen, AB24 3UE, UK

* Corresponding authors

E-mail addresses: czlicurtin@gmail.com (C.-Z. Li).

p.kechagiopoulos@abdn.ac.uk (P.N. Kechagiopoulos).

Abstract

The catalytic steam reforming of bio-ethanol will provide a sustainable route for renewable hydrogen production in a future hydrogen economy. Ni catalysts will be an economically attractive alternative to noble metals. Biochar is a promising reforming catalyst or catalyst support, having shown already good activity for tar reforming. The structure of biochar, its inherent alkali and alkaline earth metallic species and the content of O-containing functional groups are factors affecting its catalytic performance. A kinetic study of ethanol steam reforming and decomposition over a biochar-supported Ni catalyst is presented in this study in order to elucidate the role of biochar in the reaction mechanism. The effects of temperature, space velocity and reactant partial pressure were investigated over a range of conditions. The chemical structural features of used biochar samples were characterized with Raman spectroscopy. Biochar itself was found to be catalytically active and participating in ethanol reforming and decomposition. It was established that the reactions on Ni and biochar active sites were not independent. Analysis of kinetic compensation effects showed commonality on biochar and suggested that the rate-limiting step occurs in the dehydrogenation pathway on the biochar surface. O-containing functional groups in biochar were observed to reduce with reforming/decomposition time.

Keywords: Ethanol steam reforming; Nickel; Biochar; O-containing functional groups; Reaction mechanism

1. Introduction

Hydrogen is considered a clean and sustainable alternative energy carrier as it can be derived from renewable biomass [1–4]. Hydrogen has traditionally been produced from the reforming of natural gas or the gasification of coal. This however leads to high CO_2 emissions. Replacing natural gas and coal with renewable biomass-derived feedstock can contribute substantially in nullifying the environmental impact of the hydrogen production process. As such, oxygenated compounds derived from biomass have become increasingly economically appealing due to their abundance and availability. Bio-ethanol as a feedstock for the catalytic steam reforming has been researched considerably due to its attainability from diverse renewable feedstock through fermentation [5–8].

The kinetics and mechanisms of ethanol steam reforming (ESR) has been the subject of various experimental and theoretical studies, with recent reviews having discussed the current mechanistic understanding [9,10]. A common finding is that the metal catalyst promotes the scission of the C-H and C-C bonds, thus the primary mechanism is dependent on the selected metal as the catalyst.

Various metal catalysts have been investigated including Ni [11–14], Co [11], Pt [15,16], Rh [11,17,18] and Pd [19]. The consensus is that ethanol dehydrogenates, possibly forming acetaldehyde as a primary product, before C-C cleavage occurs leaving CO and CH_x precursors, which would then participate in secondary reactions; water-gas shift (WGS) and methane steam reforming (MSR). The specific dehydrogenation pathway and the level of dehydrogenation prior to C-C cleavage differs based on the metal catalyst used [20]. With minimal trade-off in activity and much higher economic feasibility, Ni has garnered attention and preference over noble metal catalysts for ESR. Early on, the isotopic work of Gates et al.

53 [21], as well as, more recently, the periodic density functional theory (DFT) calculations of
54 Wang et al. [11], describe the decomposition pathway on Ni as proceeding via initial
55 dehydrogenation towards ethoxy and further dehydrogenation towards CH_3CHO which is a
56 primary product. The C-C cleavage is likely to occur at the CH_3CHO or CH_3CO intermediates
57 [20].

58 Recent reviews presenting the progress and advances in ESR on non-noble transition
59 metals [22] and Ni specifically [23] have all highlighted the importance of promoters and
60 support materials on improving the catalyst stability and performance. Nonetheless, high-
61 performance catalysts, particularly if not noble metal based, rely many times on complex
62 formulations [24], e.g. core-shell structures, or are supported on mixed oxides, using a variety
63 of dopants, that unavoidably would increase the cost of catalyst production and the process
64 in a commercial framework.

65 Biochar is the solid product of biomass pyrolysis and/or partial gasification. Due to its low
66 cost and high porosity, it has garnered significant attention recently as a catalyst or metal
67 catalyst support for various reactions, including reforming, (trans)esterification and
68 hydrolysis [25]. The study of catalytic cracking and steam reforming of tar and its model
69 compounds using biochar-based catalysts has been a major literature focus [26],
70 demonstrating the high reforming and tar destruction activity of biochar-based catalysts [27–
71 30]. In addition, the energy value of the spent biochar can be recovered by combustion or
72 gasification further reducing energy loss and disposal cost [31–33]. Various studies have
73 further shown that the properties of intrinsic alkali and alkaline earth metallic (AAEM) species
74 in biochar contribute to its catalytic activity [33–35]. Biochar produced from pyrolysis and
75 subsequent gasification usually has a high concentration of O-containing functional groups

[36]. Previous studies have shown the importance of the O-containing functional groups to the activity of biochar [33,37].

Therefore, utilising biochar as a support material for Ni would allow the further reduction of the overall cost of the reforming process and enhance its sustainability. It can further increase the number of available sites and the available functionalities on the catalyst through the inherent content of surface oxygen containing groups and alkali and alkaline earth metals, potentially enhancing the catalyst stability. There is, however, an evident scarcity in literature with regards to the use of biochar as a catalyst or support for the steam reforming of small, non-aromatic biomass derived oxygenates and the investigation of kinetics for such reaction processes. The steam reforming of acetic acid has been studied recently on Ni/biochar [27,38], however no similar works exist for ethanol. The intrinsic kinetic effect a biochar support would possibly have on the adsorption and reaction pathway in the ethanol reforming process remains unclear.

In this work a comprehensive experimental kinetic study of ESR and ethanol decomposition over a biochar-supported Ni catalyst is presented over a range of experimental conditions in a fixed-bed reactor. Ethanol is selected as the simplest biomass-derived fuel that can allow the study of the simultaneous reactions involving hydroxyl groups and C-C bonds. The activity of biochar support during reforming was investigated and the roles of the carbon structure of biochar, inorganic AAEM species in biochar and Ni are distinguished. Unique reaction features are reported for the first time for this reaction system, including the preferential adsorption and decomposition pathways of ethanol and water on the different types of biochar sites. The possibility of interactions between the Ni and biochar active sites was also investigated. Finally, kinetic compensation effect of the

reaction system is studied for the first time detailing the wide range of energies on the Ni/biochar sites, not typically observed on traditional ESR catalysts.

2. Experimental

2.1. Sample preparation

The samples of biochar utilised were acquired from the Renergi gasification demonstration plant at Curtin University, Australia [39]. The sample was prepared from the pyrolysis and subsequent partial gasification of Mallee wood biomass. The gasification of the sample took place for a duration of 5-10 minutes at temperature of 750-850°C ensuring increased O-containing functional group concentration and in turn increased catalytic activity [31,37]. The presence of surface O-containing functional groups on these samples, specifically of aromatic $\mathrm{C-O}$ and $\mathrm{C=O}$ structures, was confirmed via X-Ray Photoelectron Spectroscopy in previous work [36]. The biochar sample was sieved to obtain two samples of particle size, ranges 106-250 µm and 55-106 µm, respectively. The elemental composition of the biochar (dry and ash-free basis) was 91.5% carbon, 1.0% hydrogen, 0.7% nitrogen and 6.8% oxygen (by difference).

The Ni/biochar catalyst with 10 wt.% Ni was prepared by the commonly applied incipient wetness impregnation method [26,27,38] using $Ni(NO_3)_2{\cdot}6H_2O$ obtained from Merck as the precursor. The water saturation volume of biochar was determined and then an aqueous solution of precursor was prepared with the same volume of water. The aqueous solution was added to the biochar sample and stirred for 4 hours before being dried in an oven at 105°C overnight. The collected catalyst sample was calcined in Ar flow (100 ml min^{-1}) with a ramp rate of 15°C min^{-1} to 600°C for 3 hours.

2.2. Reactor set up

A quartz tubular fixed-bed reactor of internal diameter 10 mm was used for the catalytic reforming and decomposition of ethanol. The catalyst bed was made up of two layers supported on a porous plate, including a layer of quartz wool to support the bed and then the Ni/biochar catalyst bed mixed with quartz sand to maintain bed height and smooth gas flow through the bed. A thermocouple was placed directly above the catalyst bed to ensure accurate temperature readings. The reactant mixture was fed by an HPLC pump. The feed was preheated using a heating tape set at 150°C prior to reactor inlet. Mass flow controllers (MFC) were used to control the flowrates of nitrogen and hydrogen gas, the former used as the carrier gas and the latter used for catalyst reduction prior to the experimental run. Connected pressure gauges were used to monitor the pressures of the gas flows.

The outlet of the reactor is connected to a three-way valve. The first outlet was connected to a HP Agilent 6890 capillary column GC equipped with pre-column backflush, a flame ionization detector (FID) and a thermal conductivity detector (TCD) for the analysis of total gaseous product range at regular intervals. The second outlet was connected to three cold traps filled with 50, 40 and 30ml of HPLC-grade $CHCl_3$/CH_3OH mixture (4:1 volume ratio) in series [40]. The traps are cooled by an ice-water bath (0°C) and two dry-ice baths (-78°C) respectively to collect liquid effluent, which was then analysed in a Agilent 6850 GC/5975B MS.

2.3. Experimental conditions and parameters

Prior to experiments the catalyst was reduced at 500°C with a stream of 5% H_2 in N_2 flow of 1 L min^{-1} for 1 h. To ensure explicit kinetic control, external mass transfer was investigated by varying the carrier gas flow rate from 0.1 to 2.5 L min^{-1} of N_2 (at 450°C and atmospheric pressure) and observing the changes in the observed reaction rate. Internal mass transfer was

investigated by varying the catalyst particle size range of the catalyst and likewise observing the changes in reaction rate. Reaction conditions were chosen to ensure that the observed reaction rates were controlled by the reaction kinetics. This necessitated conversion to be low (typically below 20%) and the operating temperature to be limited up to 450°C.

Reaction temperature was varied in the range of 300-450°C with a fixed reactant H_2O/C (C in feed) of 3 mol_{H2O}/mol_C and N_2 flow of 2 L min^{-1} at atmospheric pressure. It is important to note that initial runs were performed with no catalyst in the bed, in order to ascertain the impact of the gas phase reactions. Negligible conversion and no discernible peaks were observed from the gas phase reactions in the temperature range of 300°C to 450°C at H_2O/C ratio of 3.

The partial pressure of water was varied from 15.94 to 88.59 mbar with the partial pressure of ethanol kept at 7.91 mbar. The partial pressure variation experiments were performed at 400°C. The contact time effect was investigated by varying the reactant feed flow from 0.5 to 3.0 ml min^{-1}, corresponding to a catalyst wt./flowrate of ethanol ($W/F_{0,ethanol}$) of 58 to 349 g_{cat} s g_{eth}^{-1} (fixed catalyst weight) at 400°C with a fixed H_2O/C ratio of 3 and at atmospheric pressure. All experiments were carried out with a catalyst mass of approximately 0.1000 g.

Thermodynamic equilibrium data were obtained via the simulation of a Gibbs reactor (Gibbs free energy minimisation) in Aspen Plus software using the Peng-Robinson equation of state. The data were collected in terms of the parameters: conversion, selectivity and yield. The experimental equivalents of these parameters were calculated as shown below:

Conversion: $X_C = \frac{F_{Eth}^{In} - F_{Eth}^{Out}}{F_{Eth}^{In}} \times 100\%$

Carbon selectivity of y compound: $S_c(y) = \frac{F_y^{out}}{\sum F_{Carbon\ products}^{out}} \times 100\%$

Hydrogen yield: $Y_{H_2} = \frac{F_{H_2}^{Out}}{n \times F_{Eth}^{In}} \times 100\%$

where F^{in} and F^{out} represent inlet and outlet flowrates, respectively. n equals 6 and 3 for steam reforming and decomposition experiments, respectively.

Measured ethanol consumption rates were used to construct Arrhenius plots through the assumption of a pseudo-first-order reaction rate in ethanol partial pressure for both reforming and decomposition experiments:

$$r = kP_{Eth};\ k = Ae^{\frac{-E_a}{RT}}$$

2.4. Biochar characterization

Raman spectroscopy has been extensively implemented in characterising the chemical structure of biochar [41–44]. The structural features of the aromatic ring systems as well as the O-containing functional groups of the biochar samples obtained in this study were analysed using a Perkin-Elmer Spectrum GX FT-IR/Raman spectrometer. The procedure was adopted from the work of Li et al. [41] and has been described in detail in a previous study [42]. Briefly, 0.25 wt.% biochar sample was mixed with KBr and then ground and scanned. A baseline-corrected Raman spectrum in the range of 800-1800 cm^{-1} was fitted with 10 Gaussian bands [41]. Large aromatic ring systems with 6 or more fused benzene rings were represented by the assigned D band at 1300 cm^{-1}, while the G_R (1540 cm^{-1}), V_L (1465 cm^{-1}) and V_R (1380 cm^{-1}) bands represented the smaller aromatic ring systems containing 3-5 fused benzene rings. The total Raman peak area in the spectral range of 800-1800 cm^{-1} was used to reflect the relative content of O-containing functional groups that generate a resonance effect together with their attached aromatic ring systems.

3. Results and discussion

3.1. Ethanol steam reforming catalysed by biochar supported Ni.

Figure 1a depicts the effect of reaction temperature on ESR catalysed by Ni/biochar. The conversion of ethanol increases from 1.8% to 30% with increasing temperature from 300°C to 450°C. The hydrogen yield observed increases concurrently with conversion, with a yield of 21% obtained at 450°C. The observed selectivity trends in Figure 1b & c, are qualitatively similar to the common trends in literature for ESR catalysed by Ni [14,45–47]. The selectivity of CH_3CHO decreased while those of CO and CH_4 increased with temperature, these trends being consistent with the promotion of dehydrogenation of ethanol and decomposition of CH_3CHO as temperature increases. The selectivity of CO_2 also increased with temperature, which is consistent with the presence of some water-gas shift activity. However, when the ratio of CO/CO_2 across the temperature range is considered, the values, though decreasing with temperature, stay consistently above 1. Additionally, the observed CO/CH_4 ratio is seen to be almost constant through the temperature range at about 1.2, indicating the lack of strong secondary reaction activity to affect the decomposition products distribution. Ni is typically known to promote the water-gas shift reaction at temperatures of 400°C and above, with CO/CO_2 ratios approaching equilibrium values (0 to 0.2) at 450°C and higher, as is evidenced in the results by Zhurka et al. [14] and Vicente et al. [45] of ESR catalysed by Ni supported on inert SiO_2. It can therefore be inferred that the presence of biochar has in some way altered the reaction mechanism commonly exhibited on Ni.

The Arrhenius plot for this temperature range is shown in Figure 2, from which an apparent activation energy of about 70 kJ mol^{-1} is calculated.

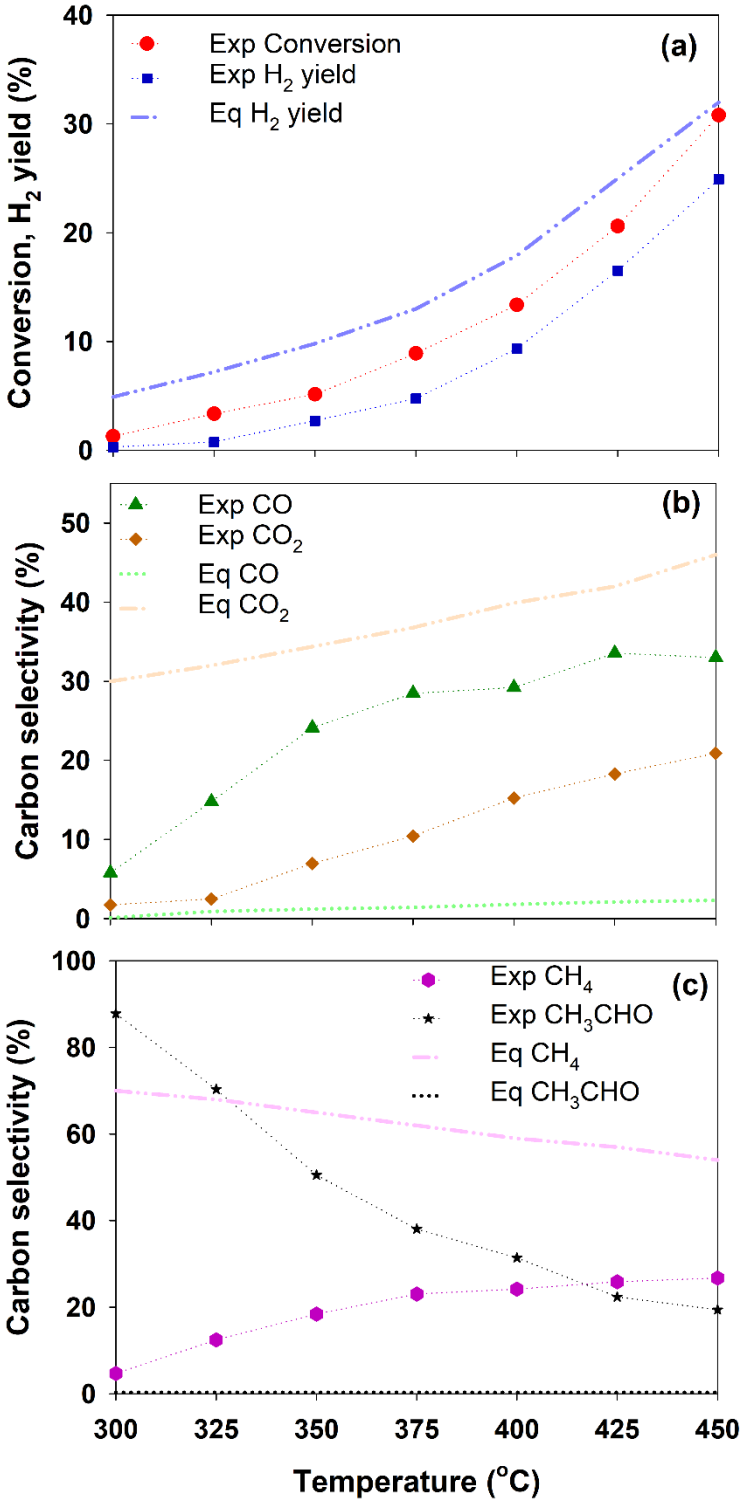

211

212 **Figure 1.** Effect of temperature on conversion and H_2 yield (a), carbon selectivities of CO & CO_2 (b) and
213 CH_4 & CH_3CHO (c) during ESR catalysed by Ni/biochar compared with equilibrium (Exp = experimental,
214 Eq = equilibrium) (S/C = 3, W/F_{Eth} = 90.9 g_{cat} s^{-1} g_{Eth} $^{-1}$).

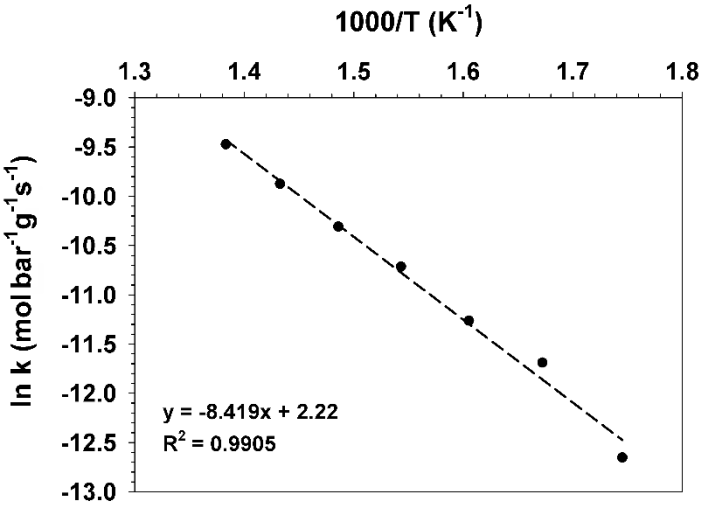

Figure 2. Arrhenius plot of ESR catalysed by Ni/biochar (S/C = 3, W/F_{Eth} = 90.9 g_{cat} s^{-1} g_{Eth} $^{-1}$).

Typically, during ethanol reforming over Ni catalyst [9,14,21], CO and CH_4 are formed from the decomposition of ethanol. The surface adsorbed precursors of CO and CH_4 undergo WGS and MSR to produce CO_2 and increase H_2 yield. In previous studies on Ni [14,45] where there exists only one type of active site and both the ethanol-derived species and the steam-derived species adsorb on the same type of site, the active species of both ethanol and steam are close enough in proximity to readily react. In this study, besides Ni, there exists two or more different types of active sites for the, possibly preferential, adsorption of ethanol-derived species and steam-derived species, including AAEM and, more importantly, O-containing functional groups on the biochar surface. Depending on reaction intermediate type, the strength of adsorption on Ni/biochar during acetic acid reforming has been seen to vary with the amount/type of O-containing functional groups [38]. H radicals on the biochar surface interacting with O-containing functional groups have been suggested to affect (reduce) tar reforming reactivity [36].

It follows then that a possible strong binding of ethanol-derived species at sites different or not in proximity to those occupied by steam-derived species would allow ethanol

derivatives to undergo dehydrogenation to CH_3CHO and decomposition towards CO and CH_4 with limited probability of further reforming and performing WGS or MSR. Another explanation could be the occurrence of a H-rich catalyst surface as a result of the dehydrogenation and decomposition reactions. This could alter the working state of the biochar surface or lead to a partial occupation of active sites through the consumption or modification of O-containing functional groups, disrupting the dynamic equilibrium of all surface species and affecting product distribution. This could also inhibit the dissociative adsorption of H_2O, leading to a scarcity of oxygen required for the promotion of secondary reactions on the surface. An abundance of surface H-species could also affect the WGS equilibrium and cause formed CO_2 to be consumed by other reactions.

The effects of varying the partial pressure of water on ethanol conversion and H_2 yield were investigated and are presented in Figure 3. The experiments were conducted at a constant overall pressure, a constant partial pressure of ethanol and a constant total volumetric flow maintained by controlling the N_2 gas flow. The conversion of ethanol is relatively constant with the observed decrease from 15.2% to 14.6% with increase in partial pressure of water being almost within acceptable error range. Figure 3 also presents the carbon selectivity of products with corresponding equilibrium selectivity data for this experiment. At high partial pressures of water, the water-gas shift reaction appears to be more promoted, with CO/CO_2 ratios below 1 and CO/CH_4 ratio decreasing as the partial pressure of water increases.

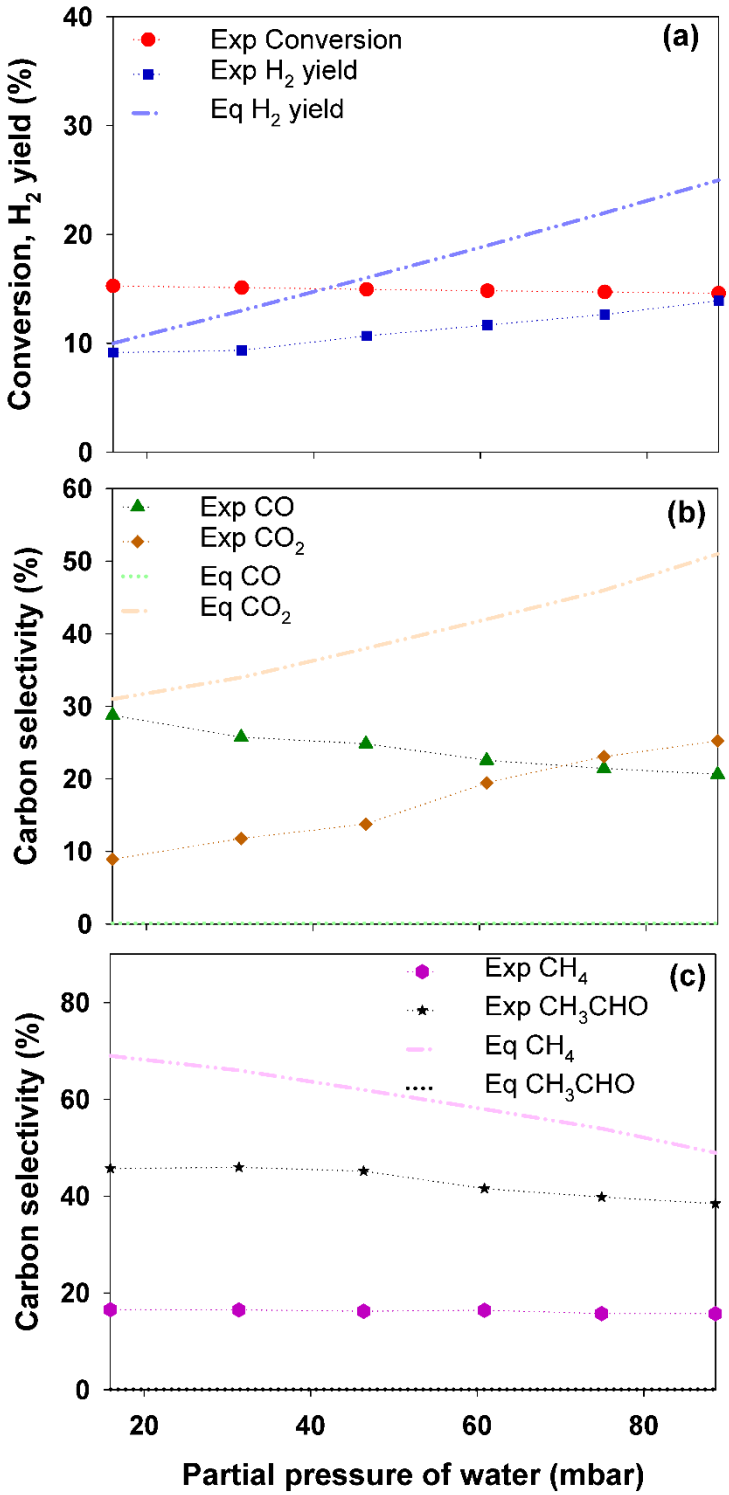

253

254 **Figure 3.** Effect of partial pressure of water on ethanol conversion and H_2 yield (a), carbon selectivities
255 of CO & CO_2 (b), CH_4 & CH_3CHO (c) during ESR catalysed by Ni/biochar compared with equilibrium at
256 400°C.

257

It follows from our initial explanation that increasing the abundance of available steam-derived surface species relative to ethanol-derived species would cause the possible spill-over and interactions to be more achievable, leading to improved WGS activity. The increased steam-derived species relative to ethanol-derived species would also mean less surface-H from dehydrogenation and decomposition reactions. Therefore, the adsorption and dissociation of H_2O on the surface would not be as hindered causing more oxygen to be available for secondary WGS reaction.

Figure 4 presents the effects of space time, depicted in terms of the W/F ratio (g_{cat} s g_{Eth}^{-1}), on the conversion of ethanol and H_2 yield at 400°C and a S/C ratio of 3. The ethanol conversion and H_2 yield as expected increased with increased contact time. A mild slope of increase was observed, likely related to the very low partial pressure of ethanol (8 mbar) resulting in low observed reaction rates. Figure 4 also shows how the selectivity towards carbon-based products evolved with changing ethanol conversion at a fixed temperature, pressure and S/C ratio with only the W/F ratio (g_{cat} s g_{Eth}^{-1}) varied. The results show that with increased contact time and conversion, there are small changes to the selectivities of the products.

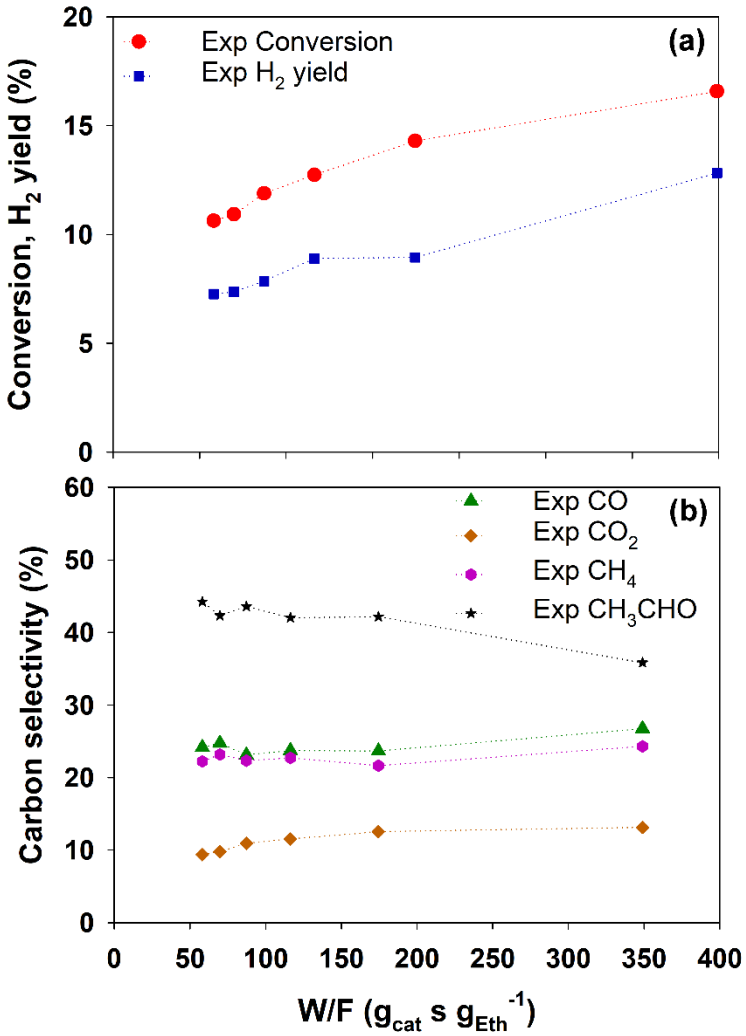

Figure 4. Effect of W/F on ethanol conversion and H_2 yield (a) and carbon selectivities of CO, CO_2, CH_4 and CH_3CHO (b) during ESR catalysed by Ni/biochar at 400°C (S/C = 3).

The observed conversion and product distribution could be due to the Ni active sites, the AAEM in biochar and/or the carbon structure of biochar. The following sections discuss results of experiments designed to distinguish the individual roles of these possible reaction sites.

3.2. Ethanol steam reforming catalysed by acid-washed biochar

To further understand the role of biochar and investigate the effects of the presence of alkali and alkaline earth metals in biochar, the effect of temperature was investigated for the ESR reaction over a sample of biochar that was acid-washed in an aqueous solution of 1M HNO_3 and then filtered and dried in a furnace overnight at 110°C. The acid-washing process

285 has been shown to lead to an effective removal of AAEM species K, Mg and Ca, reaching 90%
286 for K content reduction for similar biochar samples from mallee wood [34].

287 Figure 5 shows the effect of reaction temperature on ESR catalysed by the acid-washed
288 biochar. The conversion in this case increased from 1.1% at 300°C to 4.1% at 450°C with the
289 H_2 yield increasing from 0.2% to 2.1%. The selectivity trend shows CH_3CHO selectivity reduced
290 as temperature increased and concurrently the selectivities of CO and CH_4 increased. This
291 indicates that the dehydrogenation pathway on biochar goes through CH_3CHO, which
292 decomposed as temperature increased to form CO and CH_4. The lack of CO_2 as stated
293 previously could be attributed to the possible presence of different active sites for the ethanol
294 derivatives and the steam derivatives as well as the occurrence of H-rich surface. The
295 Arrhenius plot for the acid-washed biochar catalysed reaction in this temperature range is
296 also shown in Figure 6, from which the apparent activation energy observed is about 30 kJ
297 mol^{-1}. A more noticeable deviation from a linear fit is observed in this case, possibly due to
298 the very low conversion values and reaction rates of these experiments, however still an
299 acceptable R^2 value of 0.92 is obtained. The scatter in Figure 6 may also reflect true changes
300 in the reaction system, which are manifested in the changes in the slope of the Arrhenius plot.
301 The analytical equipment used in this study did not allow for a more accurate quantification
302 of conversion (as low as 1%) and reaction rate at the lowest temperature investigated. Further
303 investigation is warranted in the future.
304

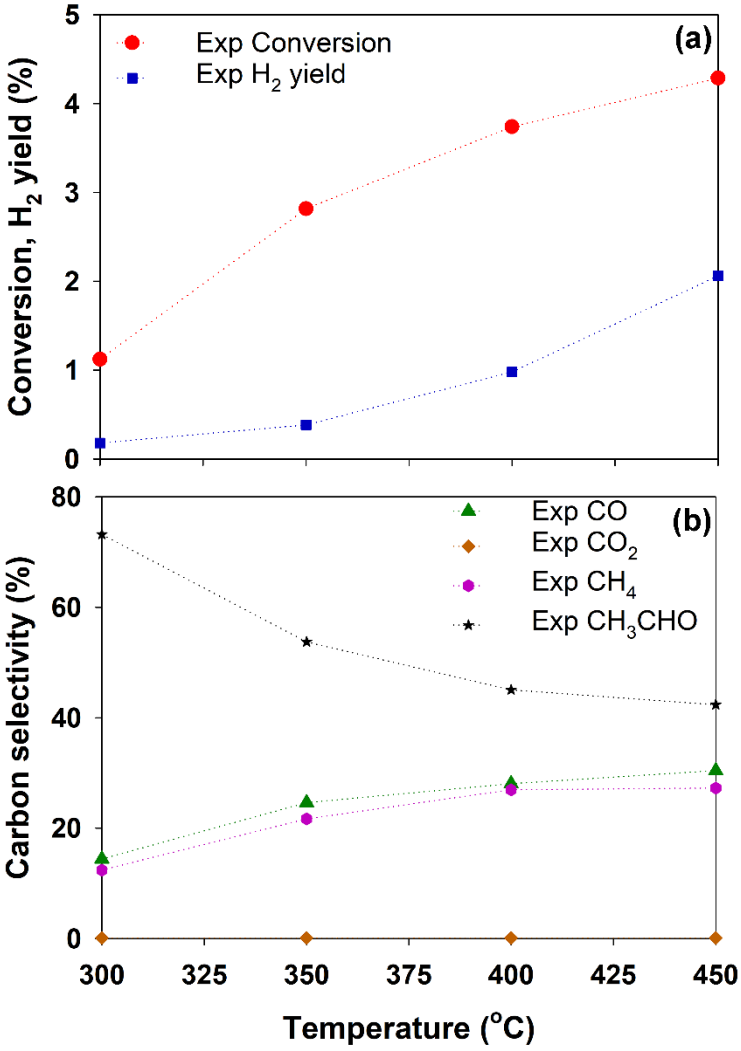

305

306 **Figure 5**. Effect of temperature on conversion, H_2 yield (a) and carbon selectivities of CO, CO_2, CH_4 &
307 CH_3CHO (b) during ESR catalysed by acid-washed biochar (S/C = 3, W/F_{Eth} = 90.9 g_{cat} s^{-1} g_{Eth} $^{-1}$).
308

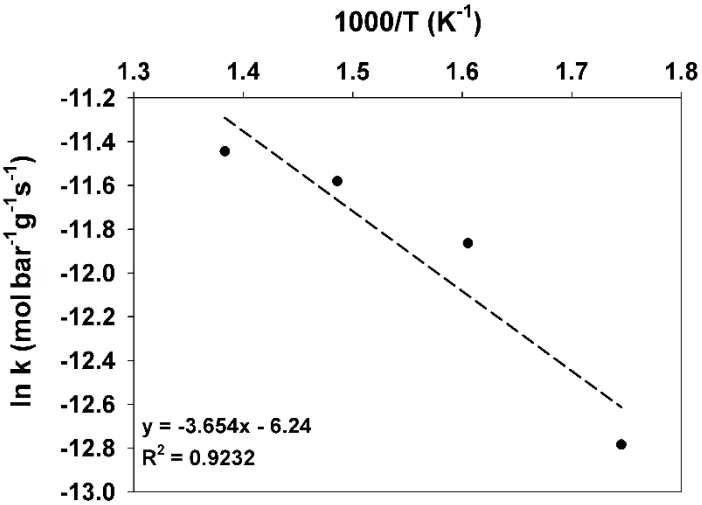

309
310 **Figure 6.** Arrhenius plot of ESR catalysed by acid-washed biochar (S/C = 3, W/F_{Eth} = 90.9 g_{cat} s^{-1} g_{Eth} $^{-1}$).
311

3.3. Ethanol steam reforming catalysed by biochar

The effect of temperature was also investigated for the ESR reaction over biochar alone as a catalyst with results shown in Figure 7. The conversion increased with temperature from 1.5% to 8.3% with H_2 yield also increasing with temperature. It is observed that at similar conversions the H_2 yield of the ESR catalysed by acid-washed biochar is less than that of the biochar catalysed reaction. The observed conversion at 300°C for both biochar and acid-washed biochar catalysts, as well as the fact that there is negligible gas phase reaction at these conditions are indicative of biochar exhibiting catalytic behaviour for ESR. The selectivity towards CH_3CHO, CH_4 and CO are all much higher than that of CO_2, and the decomposition pathway is promoted more with temperature increase as selectivity towards CH_4 and CO increase whilst that of CH_3CHO decreases.

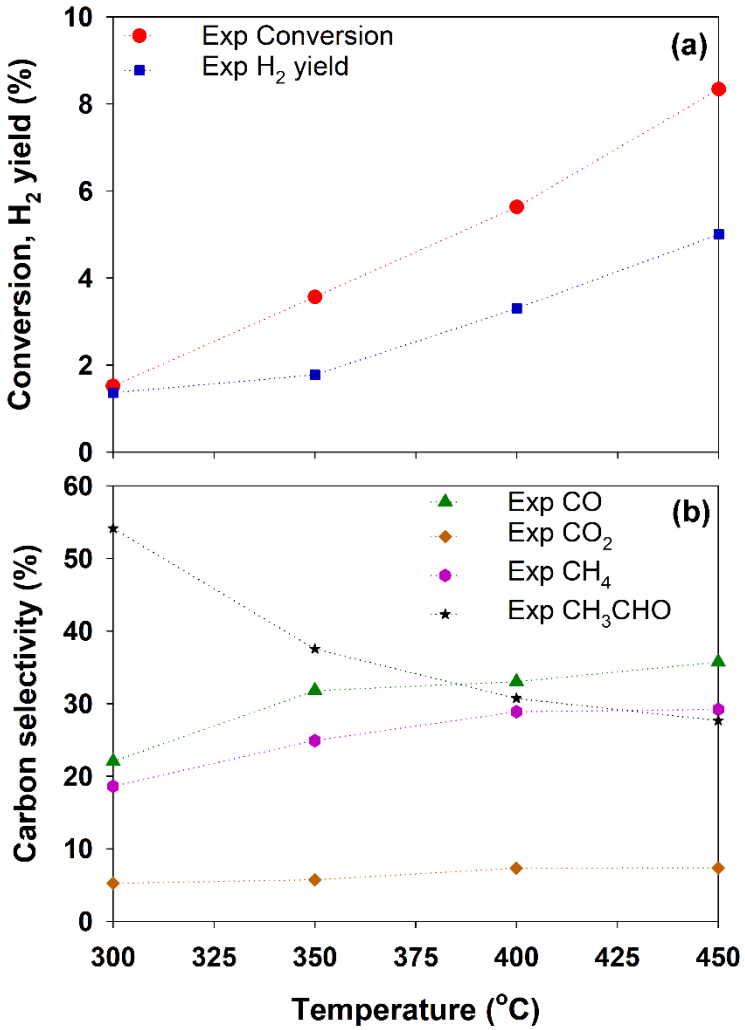

323

324 **Figure 7.** Effect of temperature on conversion and H_2 yield (top) and carbon selectivities of CO, CO_2,
325 CH_4 & CH_3CHO (bottom) during ESR catalysed by biochar (S/C = 3, W/F_{Eth} = 90.9 g_{cat} s^{-1} g_{Eth} $^{-1}$).

326

327 More CO_2 formation relative to the acid-washed-biochar-catalysed reaction products is
328 observed. The decomposition products CH_4 and CO are also more promoted over biochar,
329 therefore it could be implied that the AAEM species in biochar have additional catalytic
330 effects. The results suggest that the presence of AAEM to some extent promotes the
331 decomposition pathway leading to better conversion whilst also possibly providing additional
332 sites for the adsorption of steam derived species and consequently better WGS activity. The
333 Arrhenius plot for the biochar catalysed reaction in this temperature range is shown in Figure
334 8 from which the apparent activation energy observed is about 39 kJ mol^{-1}.

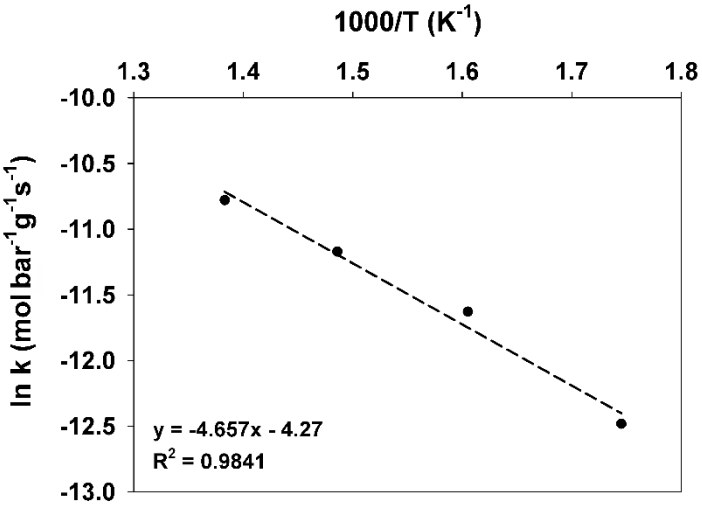

Figure 8. Arrhenius plot of ESR catalysed by biochar (S/C = 3, W/F_{Eth} = 90.9 g_{cat} s^{-1} g_{Eth} $^{-1}$).

3.4. Water-gas shift reaction catalysed by Ni/biochar

To elucidate the reason for the lack of WGS activity observed during the ESR catalysed by Ni/biochar and gain more insight into the effects of the interactions between the different active sites, WGS reaction catalysed by Ni/biochar was performed in the same temperature range 300°C to 450°C and at the same H_2O/C (C in CO) ratio of 3. The results presented in Figure 9 show that the CO conversion to CO_2 and H_2 increased from 5.4% to 72.7% as temperature increased. It is therefore evident that the Ni/biochar catalyst does not inhibit WGS reaction.

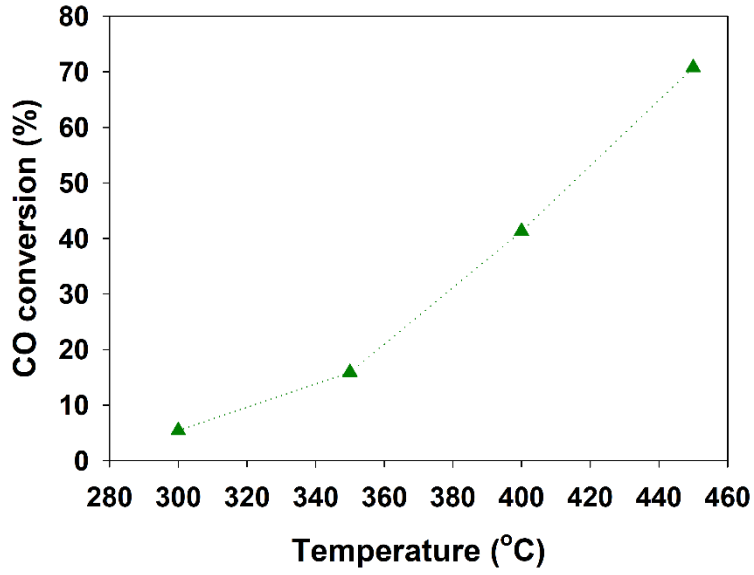

Figure 9. Effect of temperature on the conversion of CO during WGS reaction catalysed by Ni/biochar (S/C = 3, W/F_{CO} = 45.6 g_{cat} s^{-1} g_{CO} $^{-1}$).

This result supports the explanation in Section 3.1, as, in the absence of ethanol as is the case in these experiments, the catalyst surface would be significantly less H-rich. This would allow H_2O adsorption and dissociation to proceed more easily. Also, the spill-over of steam-derived species would be much easier as there are no ethanol-derived species on the catalyst surface.

3.5. Ethanol decomposition

In an attempt to gain further insight into the main reaction pathways on Ni and biochar, two temperature scan experiments were carried out to investigate the decomposition of ethanol on Ni/biochar and just biochar. Figure 10a presents the effect of temperature on the decomposition of ethanol over Ni/biochar. The carbon selectivity distribution as temperature changes is presented in Figure 10b. With no CO_2 formation whatsoever, the CH_3CHO selectivity is seen to decrease as CH_4 and CO selectivity increases steadily with increasing temperature. The carbon balance is completed by a minimal formation of C_2H_6.

The conversion/H_2 yield and carbon selectivity results of the similar experiments over a biochar catalyst are presented in Figure 10c & d respectively. The selectivity evolution shows no CO_2 once again, CO selectivity was low and decreased with temperature and CH_4 selectivity decreased in tandem with increase in C_2H_6 selectivity. As temperature increased, the formation of C_2H_6 is seen to dominate with no CH_3CHO production.

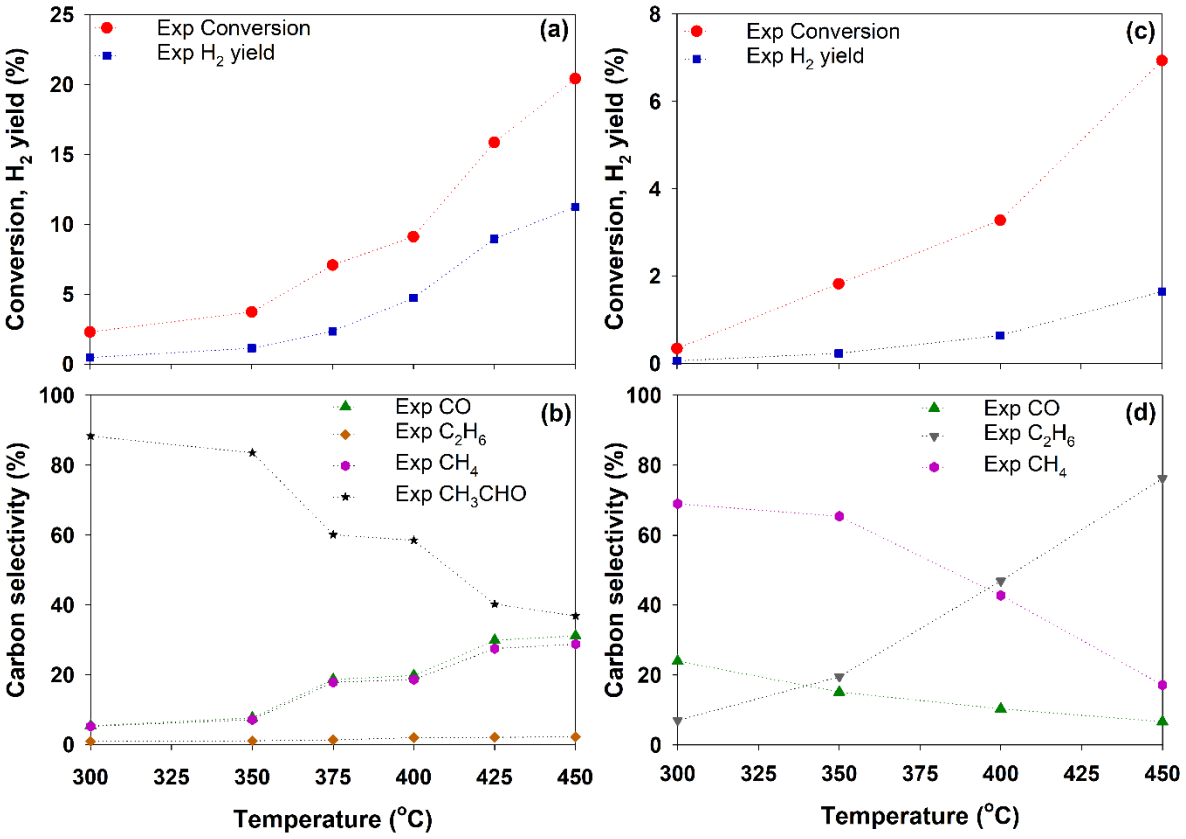

Figure 10. Ethanol decomposition conversion and H_2 yield over Ni/biochar (a), carbon selectivities of CO, C_2H_6, CH_4 and CH_3CHO over Ni/biochar (b), ethanol decomposition conversion and H_2 yield over biochar (c), carbon selectivities of CO, C_2H_6 and CH_4 over biochar (d) (S/C = 0, W/F_{Eth} = 90.9 g_{cat} s^{-1} g_{Eth}^{-1}).

A likely explanation for the C_2H_6 presence, which is not commonly encountered in ESR literature, is that a possible reaction pathway exists on biochar wherein upon adsorption the OH is cleaved from the absorbed ethanol leaving a CH_3CH_2 adsorbed ethanol derived species, which could then associatively desorb with available surface hydrogen forming C_2H_6. Alternatively, in the absence of enough hydrogen, the CH_3 produced from decomposition may

tend to recombine to give C_2H_6 rather than react with hydrogen to form CH_4. The Arrhenius plots of the decomposition reactions on Ni/biochar and biochar are presented in Figure 11.

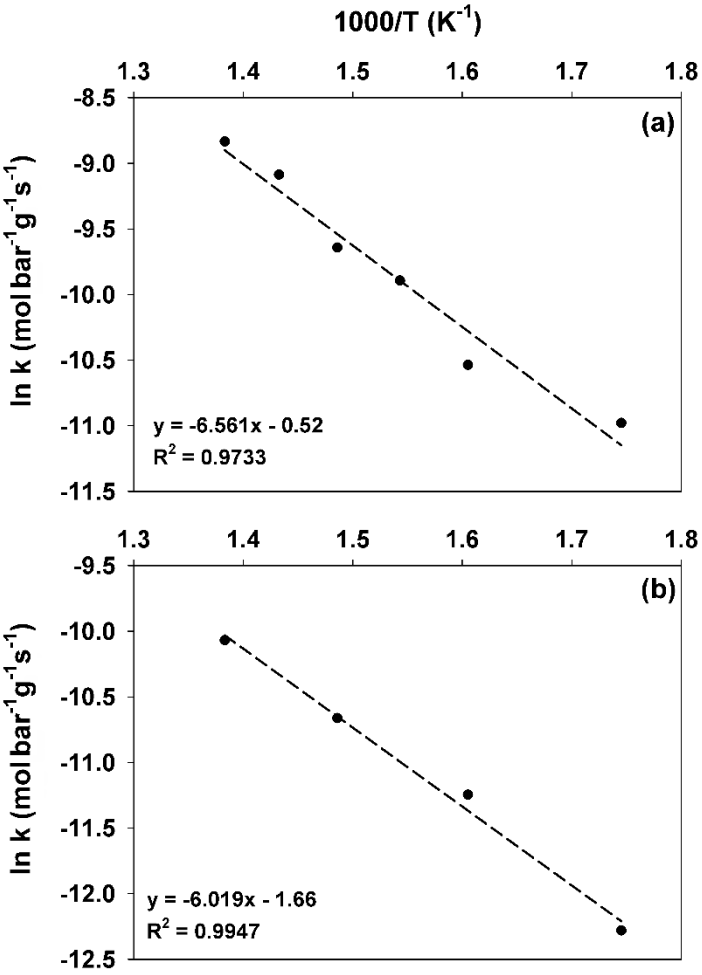

Figure 11. Arrhenius plots of ethanol decomposition catalysed by Ni/biochar (a) and biochar (b) (S/C = 0, W/F_{Eth} = 90.9 g_{cat} s^{-1} g_{Eth} $^{-1}$).

Table 1 presents a brief summary of the results of the reforming and decomposition over the different catalysts. The table shows the obtained apparent activation energies and pre-exponential factors from the Arrhenius plots, as well as the conversion and selectivity towards CH_3CHO at the minimum and maximum temperature limit examined. From the data it is conclusive that biochar is not inert and has a different reaction mechanism to that of Ni, as we observe different activation energy from the Arrhenius plots of both biochar and acid-washed biochar. If the effect of biochar alone is subtracted from the data of Ni/biochar, the

391 resulting data does not match trends observed over Ni on inert supports. We can therefore
392 conclude that the reactions on biochar and Ni active sites are not independent.

393 **Table 1.** Summary of ethanol steam reforming/decomposition results over the various catalytic
394 systems studied
395

Catalyst	Conversion at 300°C (Selectivity to CH_3CHO)	Conversion at 450°C (Selectivity to CH_3CHO)	E_a (kJ mol^{-1})	ln A (mol bar^{-1} g^{-1} s^{-1})
No catalyst (Gas phase reaction)	Not detected	Not detected	-	-
Ni/SiO_2 [14]	3% (17%)	30% (7%)	48.0	7.2
Ni/biochar	1.8% (87.8%)	30.8% (19.6%)	69.9	2.2
Biochar	1.5% (54.2%)	8.3% (27.6%)	38.7	-4.3
Acid-washed biochar	1.1% (73.2%)	4.3% (42.4%)	30.4	-6.2
Ni/biochar catalysed decomposition	2.3% (88.4%)	20.4% (36.9%)	54.6	-0.5
Biochar catalysed decomposition	0.3% (-)	6.9% (-)	50.0	-1.7

396

397 ### 3.6. Analysis of kinetic compensation effect

398 Figure 12 presents a graph of the reaction activation energies vs pre-exponential factors
399 for ethanol consumption and product formation in the experiments (steam reforming and
400 decomposition) over the different catalysts: Ni/biochar, biochar and acid-washed biochar.
401 The resulting straight-line points to evidence of the presence of some kinetic compensation
402 effect (KCE) [48].

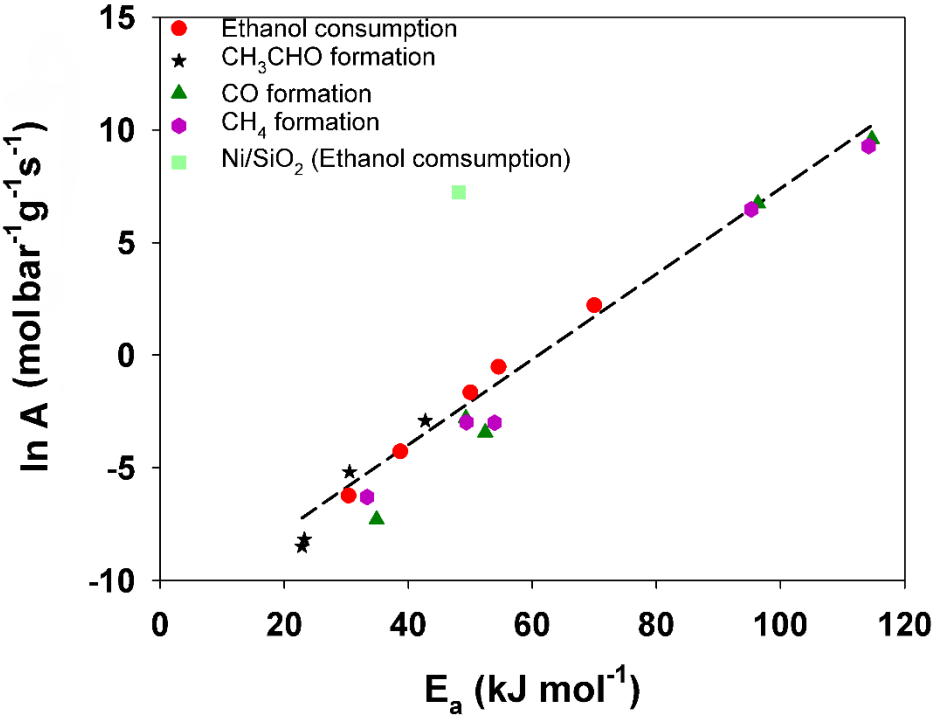

403

404 **Figure 12.** Reaction barriers vs pre-exponential factors for ethanol consumption and product
405 formation in the experiments over the different catalysts showing the presence of a kinetic
406 compensation effect. Ni/SiO_2 data obtained from [14].

407

408 To explain the existence of KCE we can consider there exists a continuum distribution of
409 active sites on a catalyst surface, some of which are more reactive than others at a given
410 temperature. With an increase in temperature the sites with high barrier for the reaction may
411 become active. Therefore, at lower temperatures the measured rate is affected mainly by
412 sites with low reaction energy barriers. At higher temperatures the measured rate is now
413 affected by both type of sites leading to a concurrent increase in the number of sites (higher
414 reaction pre-exponential factor) and the reaction barrier as both high and low energy sites
415 contribute to the measured rate (higher activation energy). In our case we have two different
416 types of sites; Ni on biochar and biochar itself. Biochar surface has a wide range of different
417 structures which would have a distribution of sites with different energies and affect the Ni-
418 biochar interactions. Therefore, Ni/biochar would also have different structures and sites

with different energies. The presence of kinetic compensation effect means that within the set of reactions a common feature is shared which could be the reactants or the catalyst [48]. In this case the commonality most likely lies in the catalyst, specifically biochar.

Understandably, the interactions of reactants, adsorbates and reaction intermediates with biochar supported metal catalysts are particularly complex and would require further investigation via advanced in situ characterisation methods in conjunction with theoretical studies to fully elucidate them. Nonetheless, given the observed trends and kinetic compensation effect it can be postulated that the reaction mechanism most logically involves ethanol and steam adsorbing on the biochar surface as illustrated in Figure 13. The organic nature of biochar allows it to offer sites with better affinity for ethanol relative to Ni [25,36,38]. In particular, the O-containing structure may be similar to those on ethanol and/or acetaldehyde, making the transition from ethanol to acetaldehyde easier. The dehydrogenation and decomposition reactions may occur on biochar sites or on sites around the Ni/biochar interface. As previously noted, typically during reforming process ethanol will first go through dehydrogenation and decomposition steps. From the KCE analysis, the decomposition and reforming reactions share the same commonality and it can be extrapolated that the rate limiting step occurs on biochar within the dehydrogenation pathway.

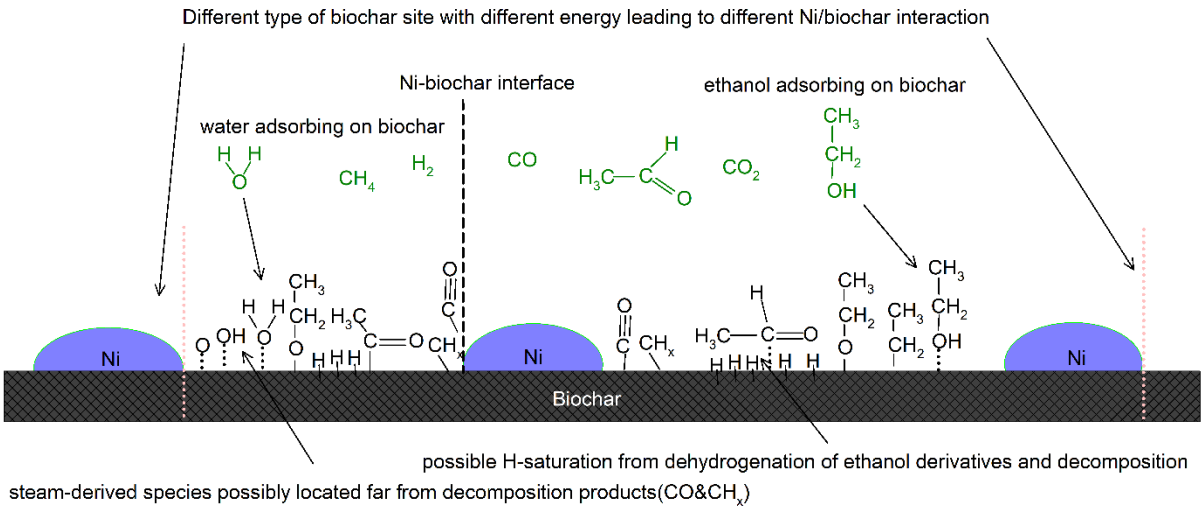

438

439 **Figure 13.** Schematic view of postulated distribution of ethanol and steam derived species on various
440 active sites on Ni/biochar during the reforming reaction.

441

442 ## 3.7. Raman spectroscopic characterization of biochar

443 Samples from the ESR process over Ni/biochar and just biochar at S/C ratio of 3 and 450°C,
444 as well as samples from the ethanol decomposition experiments over Ni/biochar and biochar
445 at S/C ratio of 0 and 450°C were characterized via Raman spectroscopy. For each experiment,
446 two different reaction times were used, namely 30 mins and 60 mins, noting that there was
447 little to no discernible change in the reaction rate for both reaction times. Spectra from raw
448 biochar as well as fresh Ni/biochar catalyst after reduction in H_2 were also collected for
449 comparison. The Raman spectra of all biochar samples in the range of 800-1800 cm^{-1} are
450 presented in Figure S1 in the Supporting Information. These spectra were curve fitted by 10
451 Gaussian peaks, as described in the work of Li et al. [41,42]. An example Raman spectrum
452 deconvolution is shown in Figure S2 of the Supporting Information, evidencing the successful
453 spectrum curve-fitting with these bands. The total Raman peak areas for these biochar
454 samples are shown in Figure 14.

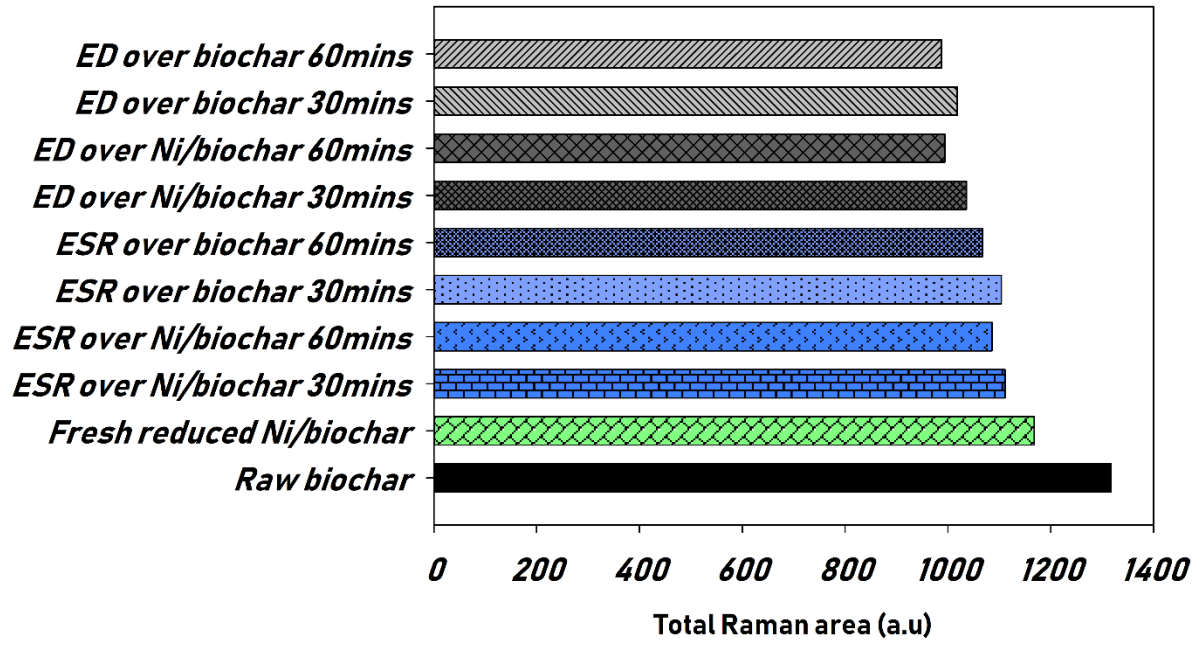

455

456 **Figure 14.** Raman spectroscopic data showing total Raman peak area (800 - 1800 cm^{-1}) of biochar
457 samples obtained from ESR (ethanol steam reforming) and ED (ethanol decomposition) experiments
458 at 450°C at different reaction times, in comparison to that of raw biochar and fresh reduced
459 Ni/biochar.

460

461 After reforming and decomposition reactions the total Raman peak area in all biochar
462 samples decreased, indicating the consumption of the O-containing functional groups when
463 biochar is used as a catalyst. When comparing the Ni/biochar catalysed and biochar catalysed
464 ESR samples, the depletion of O-containing functional groups content with reaction time is
465 found to be similar at approximately 8.5% over the 30-60 min reaction interval. This could be
466 implying that the biochar is similarly active even when used as a support and the ethanol and
467 steam preferentially adsorb on biochar active sites. In addition, when comparing the samples
468 from the ethanol decomposition experiments over Ni/biochar and biochar, the Raman area
469 depletion values are also similar at roughly 15% over the 30-60 min reaction interval. Again,
470 this possibly implies that even in the case where only ethanol and ethanol derived species are
471 present, they preferentially adsorb on biochar active sites.

It is further noted in the previous data that Raman peak area reduction during decomposition is larger than during ESR. This is further elaborated in Table 2 showing the reduction of total Raman peak area as the S/C ratio is increased at 400°C over Ni/biochar, and the respective H_2 yield and CO and CO_2 selectivities for these experiments. The total Raman peak area which relates to the content of O-containing functional groups is observed to reduce at a lower rate with increasing abundance of H_2O, indicating that the presence of steam facilitates the replenishment or maintenance of the O-containing functional groups on the biochar surface. These findings are in good agreement with previous studies where steam has been used to activate biochar and increase the surface-O functionality [25,36,49], and suggest that the catalytic activity of Ni/biochar is linked with and can be enhanced by the presence of O-containing functional groups, as also evidenced by the increasing H_2 yield and CO_2 selectivity values in Table 2.

Table 2. Relative change in total Raman peak area (800 - 1800 cm^{-1}) over the 30-60 min reaction interval of biochar samples obtained from experiments varying S/C ratio at 400°C over Ni/biochar and respective products formation.

Reaction conditions	Total Raman peak area change (%)	CO_2 selectivity (%)	CO selectivity (%)	H_2 yield (%)
Ethanol decomposition	-14.69	0	20.81	4.72
ESR at S/C = 1	-13.23	8.89	28.78	9.14
ESR at S/C = 3	-8.33	13.76	24.61	10.67
ESR at S/C = 6	-3.45	25.35	20.12	14.11

4. Conclusions

Ethanol steam reforming and decomposition experiments over a wide range of conditions were carried out over Ni/biochar, biochar and acid-washed biochar catalysts in an attempt to ascertain the overall reaction mechanism and the effect of the biochar support on the latter.

The observed results show that biochar is catalytically active during reforming and decomposition and follows a different mechanism from that of Ni. The AAEM in biochar contribute to the observed catalytic effect of biochar. The reactions on the active sites of biochar and Ni are not independent. Low CO_2 formation was observed during the ESR over all catalysts. This was not the case during independent WGS kinetic experiments over Ni/biochar, suggesting that, during ESR, WGS is hindered possibly by coverage effects or changes in the working state of the catalyst surface induced from the adsorption and dehydrogenation of ethanol.

The decomposition of ethanol on biochar in the absence of steam interestingly showed the formation of C_2H_6 species, which could be a result of the abstraction of the OH group forming an ethyl CH_3CH_2 surface species which would associatively desorb with available hydrogen. It could also be as a result of the CH_3 species formed from decomposition recombining to C_2H_6 due to lack of sufficient hydrogen to form CH_4. Kinetic compensation effect was observed with a possible rate limiting step on biochar being common to all reactions. The Raman spectroscopy results show similar reduction in O-containing functional groups when biochar is used alone or as a support to Ni, while the presence of H_2O in both cases helps maintain the population of these groups.

Acknowledgements

This research received funding from the Australian Government through the Australian Research Council (project number: DP180101788) and through ARENA's Emerging Renewables Program. This work was also supported by the Aberdeen-Curtin Alliance. We wish to thank Li Dong, Shu Zhang and Yao Song for providing raw biochar, and Richard Gunawan and Zhitao Wang for assistance during rig set-up.

References

[1] P. Nikolaidis, A. Poullikkas, A comparative overview of hydrogen production processes, Renew. Sustain. Energy Rev. 67 (2017) 597–611.

[2] M. Ni, D.Y.C. Leung, M.K.H. Leung, A review on reforming bio-ethanol for hydrogen production, Int. J. Hydrogen Energy. 32 (2007) 3238–3247.

[3] N. Sanchez, R.Y. Ruiz, B. Cifuentes, M. Cobo, Hydrogen from glucose: A combined study of glucose fermentation, bioethanol purification, and catalytic steam reforming, Int. J. Hydrogen Energy. 41 (2016) 5640–5651.

[4] P.D. Vaidya, A.E. Rodrigues, Insight into steam reforming of ethanol to produce hydrogen for fuel cells, Chem. Eng. J. 117 (2006) 39–49.

[5] C.. Rioche, S.. Kulkarni, M.. Meunier, J.. Breen, R.. Burch, Steam reforming of model compounds and fast pyrolysis bio-oil on supported noble metal catalysts, Appl. Catal. B Environ. 61 (2005) 130–139.

[6] R. González-Gil, I. Chamorro-Burgos, C. Herrera, M.A. Larrubia, M. Laborde, F. Mariño, L.J. Alemany, Production of hydrogen by catalytic steam reforming of oxygenated model compounds on Ni-modified supported catalysts. Simulation and experimental study, Int. J. Hydrogen Energy. 40 (2015) 11217–11227.

[7] R. Trane, S. Dahl, M.S. Skjøth-Rasmussen, A.D. Jensen, Catalytic steam reforming of bio-oil, Int. J. Hydrogen Energy. 37 (2012) 6447–6472.

[8] L. V Mattos, G. Jacobs, B.H. Davis, F.B. Noronha, Production of hydrogen from ethanol: Review of reaction mechanism and catalyst deactivation, Chem. Rev. 112 (2012) 4094–4123.

[9] D. Zanchet, J.B.O. Santos, S. Damyanova, J.M.R. Gallo, J.M.C. Bueno, Toward understanding metal-catalyzed ethanol reforming, ACS Catal. 5 (2015) 3841–3863.

[10] K.D. Punase, N. Rao, P. Vijay, A review on mechanistic kinetic models of ethanol steam reforming for hydrogen production using a fixed bed reactor, Chem. Pap. 73 (2019) 1027–1042.

[11] J.H. Wang, C.S. Lee, M.C. Lin, Mechanism of ethanol reforming: Theoretical foundations, J. Phys. Chem. C. 113 (2009) 6681–6688.

[12] I. Llera, V. Mas, M.L. Bergamini, M. Laborde, N. Amadeo, Bio-ethanol steam reforming on Ni based catalyst. Kinetic study, Chem. Eng. Sci. 71 (2012) 356–366.

[13] A. Akande, A. Aboudheir, R. Idem, A. Dalai, Kinetic modeling of hydrogen production by the catalytic reforming of crude ethanol over a co-precipitated Ni-Al_2O_3 catalyst in a packed bed tubular reactor, Int. J. Hydrogen Energy. 31 (2006) 1707–1715.

[14] M.D. Zhurka, A.A. Lemonidou, J.A. Anderson, P.N. Kechagiopoulos, Kinetic analysis of the steam reforming of ethanol over Ni/SiO_2 for the elucidation of metal-dominated reaction pathways, React. Chem. Eng. 3 (2018) 883–897.

[15] R. Alcalá, M. Mavrikakis, J.A. Dumesic, DFT studies for cleavage of C-C and C-O bonds in surface species derived from ethanol on Pt(111), J. Catal. 218 (2003) 178–190.

[16] F. Soyal-Baltacioğlu, A.E. Aksoylu, Z.I. Önsan, Steam reforming of ethanol over Pt-Ni Catalysts, Catal. Today. 138 (2008) 183–186.

[17] S. Cavallaro, Ethanol Steam Reforming on Rh/Al_2O_3 Catalysts, Energy and Fuels. 14 (2000) 1195–1199.

[18] J. Zhang, Z. Zhong, X.M. Cao, P. Hu, M.B. Sullivan, L. Chen, Ethanol steam reforming on rh catalysts: Theoretical and experimental understanding, ACS Catal. 4 (2014) 448–456.

[19] M. Li, W. Guo, R. Jiangs, L. Zhao, H. Shan, Decomposition of ethanol on Pd(111): A

561 density functional theory stutdy, Langmuir. 26 (2010) 1879–1888.
562 [20] J.E. Sutton, D.G. Vlachos, Ethanol activation on closed-packed surfaces, Ind. Eng.
563 Chem. Res. 54 (2015) 4213–4225.
564 [21] S.M. Gates, J.N. Russell Jr., J.T. Yates Jr., Bond activation sequence observed in the
565 chemisorption and surface reaction of ethanol on Ni(111), Surf. Sci. 171 (1986) 111–
566 134.
567 [22] S. Ogo, Y. Sekine, Recent progress in ethanol steam reforming using non-noble
568 transition metal catalysts: A review, Fuel Process. Technol. 199 (2020) 106238.
569 [23] T.K. Phung, T.L.M. Pham, A.N.T. Nguyen, K.B. Vu, H.N. Giang, T.A. Nguyen, T.C. Huynh,
570 H.D. Pham, Effect of Supports and Promoters on the Performance of Ni-Based
571 Catalysts in Ethanol Steam Reforming, Chem. Eng. Technol. 43 (2020) 672–688.
572 [24] V. Palma, C. Ruocco, M. Cortese, M. Martino, Bioalcohol Reforming: An Overview of
573 the Recent Advances for the Enhancement of Catalyst Stability, Catalysts. 10 (2020).
574 [25] R. Shan, J. Han, J. Gu, H. Yuan, B. Luo, Y. Chen, A review of recent developments in
575 catalytic applications of biochar-based materials, Resour. Conserv. Recycl. 162 (2020)
576 105036.
577 [26] J. Ashok, N. Dewangan, S. Das, P. Hongmanorom, M.H. Wai, K. Tomishige, S. Kawi,
578 Recent progress in the development of catalysts for steam reforming of biomass tar
579 model reaction, Fuel Process. Technol. 199 (2020) 106252.
580 [27] J. Chen, M. Wang, S. Wang, X. Li, Hydrogen production via steam reforming of acetic
581 acid over biochar-supported nickel catalysts, Int. J. Hydrogen Energy. 43 (2018)
582 18160–18168.
583 [28] D. Buentello-Montoya, X. Zhang, J. Li, V. Ranade, S. Marques, M. Geron, Performance
584 of biochar as a catalyst for tar steam reforming: Effect of the porous structure, Appl.
585 Energy. 259 (2020) 114176.
586 [29] L. Ren, L.J. Yan, Y.H. Bai, Y. Liu, P. Lv, Y.X. Wang, F. Li, Effects of loading methods and
587 oxidation degree of support on the tar reforming activity of char-supported Ni
588 catalyst using toluene as a model compound, Fuel Process. Technol. 201 (2020)
589 106347.
590 [30] C. Quan, H. Wang, N. Gao, Development of activated biochar supported Ni catalyst
591 for enhancing toluene steam reforming, Int. J. Energy Res. 44 (2020) 5749–5764.
592 [31] Z. Min, P. Yimsiri, M. Asadullah, S. Zhang, C.Z. Li, Catalytic reforming of tar during
593 gasification. Part II. Char as a catalyst or as a catalyst support for tar reforming, Fuel.
594 90 (2011) 2545–2552.
595 [32] Y. Song, Y. Zhao, X. Hu, L. Zhang, S. Sun, C.Z. Li, Destruction of tar during volatile-char
596 interactions at low temperature, Fuel Process. Technol. 171 (2018) 215–222.
597 [33] Y. Song, Y. Wang, X. Hu, S. Hu, J. Xiang, L. Zhang, S. Zhang, Z. Min, C.Z. Li, Effects of
598 volatile-char interactions on in situ destruction of nascent tar during the pyrolysis and
599 gasification of biomass. Part I. Roles of nascent char, Fuel. 122 (2014) 60–66.
600 [34] S. Zhang, Y. Song, Y.C. Song, Q. Yi, L. Dong, T.T. Li, L. Zhang, J. Feng, W.Y. Li, C.Z. Li, An
601 advanced biomass gasification technology with integrated catalytic hot gas cleaning.
602 Part III: Effects of inorganic species in char on the reforming of tars from wood and
603 agricultural wastes, Fuel. 183 (2016) 177–184.
604 [35] C. Xu, Z.-Y. Du, S.-Q. Yang, H.-D. Ma, J. Feng, Effects of Inherent Potassium on the
605 Catalytic Performance of Ni/Biochar for Steam Reforming of Toluene as a Tar Model
606 Compound, Chinese J. Chem. Eng. (2020) 108653.
607 [36] Y. Liu, M. Paskevicius, H. Wang, G. Parkinson, J.P. Veder, X. Hu, C.Z. Li, Role of O-

containing functional groups in biochar during the catalytic steam reforming of tar using the biochar as a catalyst, Fuel. 253 (2019) 441–448.
[37] Z. Min, S. Zhang, P. Yimsiri, Y. Wang, M. Asadullah, C.Z. Li, Catalytic reforming of tar during gasification. Part IV. Changes in the structure of char in the char-supported iron catalyst during reforming, Fuel. 106 (2013) 858–863.
[38] Y. Wang, Z. Zhang, S. Zhang, Y. Wang, S. Hu, J. Xiang, X. Hu, Steam reforming of acetic acid over Ni/biochar catalyst treated with HNO3: Impacts of the treatment on surface properties and catalytic behaviors, Fuel. 278 (2020) 118341.
[39] Advanced biomass gasification technology, Australian Renewable Energy Agency. https://arena.gov.au/projects/advanced-biomass-gasification-technology/. (accessed October 28, 2019), (2018) 1–13.
[40] Z. Min, M. Asadullah, P. Yimsiri, S. Zhang, H. Wu, C.Z. Li, Catalytic reforming of tar during gasification. Part I. Steam reforming of biomass tar using ilmenite as a catalyst, Fuel. 90 (2011) 1847–1854.
[41] X. Li, J. Hayashi, C.Z. Li, FT-Raman spectroscopic study of the evolution of char structure during the pyrolysis of a Victorian brown coal, Fuel. 85 (2006) 1700–1707.
[42] X. Li, J. Hayashi, C.Z. Li, Volatilisation and catalytic effects of alkali and alkaline earth metallic species during the pyrolysis and gasification of Victorian brown coal. Part VII. Raman spectroscopic study on the changes in char structure during the catalytic gasification in air, Fuel. 85 (2006) 1509–1517.
[43] H.L. Tay, S. Kajitani, S. Zhang, C.Z. Li, Inhibiting and other effects of hydrogen during gasification: Further insights from FT-Raman spectroscopy, Fuel. 116 (2014) 1–6.
[44] H.L. Tay, S. Kajitani, S. Zhang, C.Z. Li, Effects of gasifying agent on the evolution of char structure during the gasification of Victorian brown coal, in: Fuel, Elsevier Ltd, 2013: pp. 22–28.
[45] J. Vicente, J. Ereña, C. Montero, M.J. Azkoiti, J. Bilbao, A.G. Gayubo, Reaction pathway for ethanol steam reforming on a Ni/SiO2 catalyst including coke formation, Int. J. Hydrogen Energy. 39 (2014) 18820–18834.
[46] J. Comas, F. Marino, M. Laborde, N. Amadeo, Bio-ethanol steam reforming on Ni/Al2O3 catalyst, Chem. Eng. J. 98 (2004) 61–68.
[47] P. Biswas, D. Kunzru, Steam reforming of ethanol for production of hydrogen over Ni/CeO_2 - ZrO_2, Int. J. Hydrogen Energy. 32 (2007) 969–980.
[48] B. V. L'vov, A.K. Galwey, Interpretation of the kinetic compensation effect in heterogeneous reactions: Thermochemical approach, Int. Rev. Phys. Chem. 32 (2013) 515–557.
[49] Y. Liu, M. Paskevicius, H. Wang, C. Fushimi, G. Parkinson, C.Z. Li, Difference in tar reforming activities between biochar catalysts activated in H_2O and CO_2, Fuel. 271 (2020) 117636.